Astronomy & Astrophysics manuscript no. 29460
October 19, 2016
©ESO 2016

arXiv:1610.05322v1 [astro-ph.GA] 17 Oct 2016

Hot methanol from the inner region of the HH 212 protostellar system

S. Leurini[1], C. Codella[2], S. Cabrit[3], F. Gueth[4], A. Giannetti[1], F. Bacciotti[2], R. Bachiller[5], C. Ceccarelli[6], A. Gusdorf[7], B. Lefloch[6], L. Podio[2], and M. Tafalla[5]

[1] Max-Planck-Institut für Radioastronomie, Auf dem Hügel 69, D-53121, Bonn, Germany
e-mail: sleurini@mpifr.de
[2] INAF, Osservatorio Astrofisico di Arcetri, Largo E. Fermi 5, 50125 Firenze, Italy
[3] LERMA, Observatoire de Paris, PSL Research University, CNRS, Sorbonne Universités, UPMC Univ. Paris 06, École Normale Supérieure, F-75014, Paris, France
[4] IRAM, 300 rue de la Piscine, 38406 Saint Martin d'Hères, France
[5] IGN, Observatorio Astronómico Nacional, Alfonso XII 3, 28014 Madrid, Spain
[6] Univ. Grenoble Alpes, CNRS, IPAG, F-38000, Grenoble, France
[7] LERMA, Département de physique de l'ENS, ENS, Observatoire de Paris, PSL Research University, Université Cergy-Pontoise, Université Paris Seine, Sorbonne Universités, UPMC Univ Paris 06, CNRS, Paris France

ABSTRACT

The mechanisms leading to the formation of disks around young stellar objects (YSOs) and to the launching of the associated jets are crucial to the understanding of the earliest stages of star and planet formation. HH 212 is a privileged laboratory to study a pristine jet-disk system. Therefore we investigate the innermost region (< 100 AU) around the HH 212-MM1 protostar through ALMA band 7 observations of methanol. The 8 GHz bandwidth spectrum towards the peak of the continuum emission of the HH 212 system reveals at least 19 transitions of methanol. Several of these lines (among which several vibrationally excited lines in the $v_t = 1, 2$ states) have upper energies above 500 K. They originate from a compact (< 135 AU in diameter), hot (∼ 295 K) region elongated along the direction of the SiO jet. We performed a fit in the *uv* plane of various velocity channels of the strongest high-excitation lines. The blue- and red-shifted velocity centroids are shifted roughly symmetrically on either side of the jet axis, indicating that the line-of-sight velocity beyond 0.7 km s^{-1} from systemic is dominated by rotational motions. The velocity increases moving away from the protostar further indicating that the emission of methanol is not associated with a Keplerian disk or rotating-infalling cavity, and it is more likely associated with outflowing gas. We speculate that CH_3OH traces a disk wind gas accelerated at the base. The launching region would be at a radius of a few astronomical units from the YSO.

Key words. stars: formation / ISM: jets and outflows / ISM: molecules / ISM: individual objects: HH 212

1. Introduction

The Class 0 protostellar stages are clearly associated with mass loss and in particular with fast collimated jets, usually observed as extremely high-velocity structures in CO and SiO transitions. In contrast, the evidence of disks in these very early phases of evolution is much less clear. Magnetic fields play a fundamental role in regulating the formation of young stellar objects (YSO) and of the disk as they are believed to remove the excess angular momentum from the infalling material allowing accretion onto the central object. However, this "magnetic braking" is so efficient that Keplerian disks may be initially suppressed beyond 10 AU (Price & Bate 2007). The expected small sizes of disks in Class 0 phases and the fact that in these still deeply embedded objects the emission of the surrounding envelope is likely entangled with that of the disk make the detection of Keplerian disks in Class 0 YSOs very challenging (e.g. Lee et al. 2009; Tobin et al. 2012) even in the ALMA era (e.g. Murillo et al. 2013; Sakai et al. 2014; Ohashi et al. 2014).

HH 212 is a strikingly bright and symmetric bipolar jet from a Class 0 source at a distance of 450 pc extensively observed with IRAM PdBI, SMA, and ALMA (Lee et al. 2006, 2007; Codella et al. 2007; Cabrit et al. 2007; Lee et al. 2008; Cabrit et al. 2012; Codella et al. 2014; Lee et al. 2015; Podio et al. 2015). A disk was observed with ALMA towards the HH 212–MM1 protostar in HCO^+, $C^{17}O$, and SO emission with velocity gradients along the equatorial plane consistent with a rotating disk of $\simeq 0\farcs2 = 90$ AU in radius around a $\simeq 0.2-0.3 M_\odot$ source. Therefore, the HH 212 region is, to our knowledge, the only example of a protostellar region with a bright bipolar jet and a compact rotating disk, and is thus a privileged laboratory to study a pristine jet-disk system. The asymmetric line profile of one high-excitation (∼300 K) HDO transition recently observed towards HH 212–MM1 (Codella et al. 2016) suggests the possible occurrence of hot and expanding gas associated with a disk wind, calling for further multiline observations.

In this Letter, we further exploit ALMA Band 7 data (from Codella et al. 2014) to investigate the inner 100 AU of the HH 212 system through a survey of methanol (CH_3OH) high-energy lines (up to $E_u = 747$ K). High-excitation lines of CH_3OH probe the innermost gas around the protostar (e.g. Leurini et al. 2007a; Maret et al. 2014) and can be used as a selective tracer of the kinematics of the region.

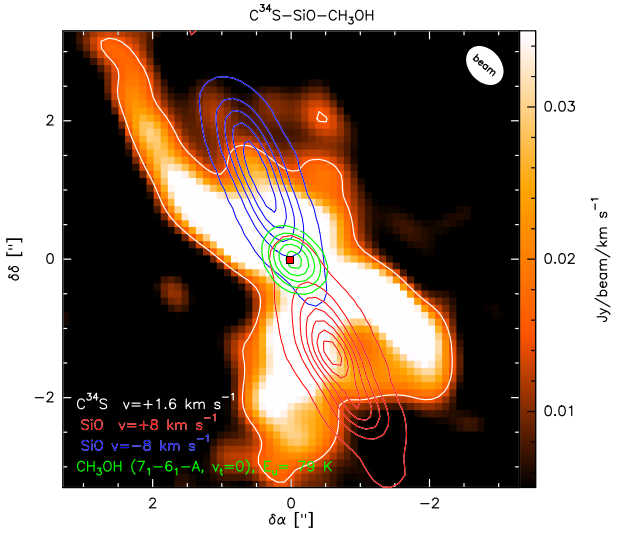

Fig. 1. The HH 212 protostellar system as observed by ALMA (Codella et al. 2014). The colour scale represents the $C^{34}S$ (7–6) emission close to the systemic velocity (the white contour is the 5 σ level). Blue and red contours show the blue- and red-shifted SiO(8–7) jet at ± 8 km s^{-1} from the systemic velocity. Green contours show the integrated emission of the $7_1 - 6_1$-$A, v_t = 0$ CH_3OH line (from 10 σ, 90 mJy beam^{-1} km^{-1} s, in steps of 10 σ). The red square marks the peak of the continuum emission (Lee et al. 2014). The filled ellipse shows the synthesised beam.

2. Observations

The data presented are part of the observations discussed by Codella et al. (2014), Podio et al. (2015), and Codella et al. (2016). We refer to these papers for further details and give here a short summary of the observations. HH 212 was observed in Band 7 during the cycle 0 phase of ALMA. The data cover the frequencies 333.7–337.4 GHz and 345.6–349.3 GHz with a spectral resolution of 488 kHz (corresponding to 0.42–0.44 km s^{-1}). The continuum-subtracted images have a typical clean-beam FWHM of 0.″6 × 0.″5 (PA $\simeq$ 40°), and an rms noise level of 3 mJy beam^{-1} in the 488 kHz channel. Positions are given with respect to the continuum peak (α(J2000) = 05^h 43^m 51.s41, δ(J2000) = –01° 02′ 53.″17, Lee et al. 2014).

3. Results

The HH 212 protostellar system is shown in Fig. 1. We identified 19 lines of CH_3OH in the 8 GHz bandwidth spectrum towards the 0.9 mm continuum peak (see Figs. 2 and A.1 for the full spectrum) using the Weeds package (Maret et al. 2011) and the spectroscopic parameters from the Jet Propulsion Laboratory (JPL) molecular database (Pickett et al. 1998). Typical line-widths are 4–5 km s^{-1}. The identified lines are in Table A.1 and they belong to the first three vibrational states: nine lines in the $v_t = 0$ level, one in $v_t = 1$, and nine in $v_t = 2$, respectively. To our knowledge, $v_t = 1$ CH_3OH lines around low-mass YSOs were previously reported only around the Class 0 protostar NGC 1333–IRAS2A (Maret et al. 2014; Maury et al. 2014). The lines cover a wide excitation range (E_u ~79 K to 747 K) and they sample the high-excitation regime well (eight transitions have $E_u > 500$ K). These data therefore offer a unique opportunity to investigate the nature of the hot gas surrounding the protostar.

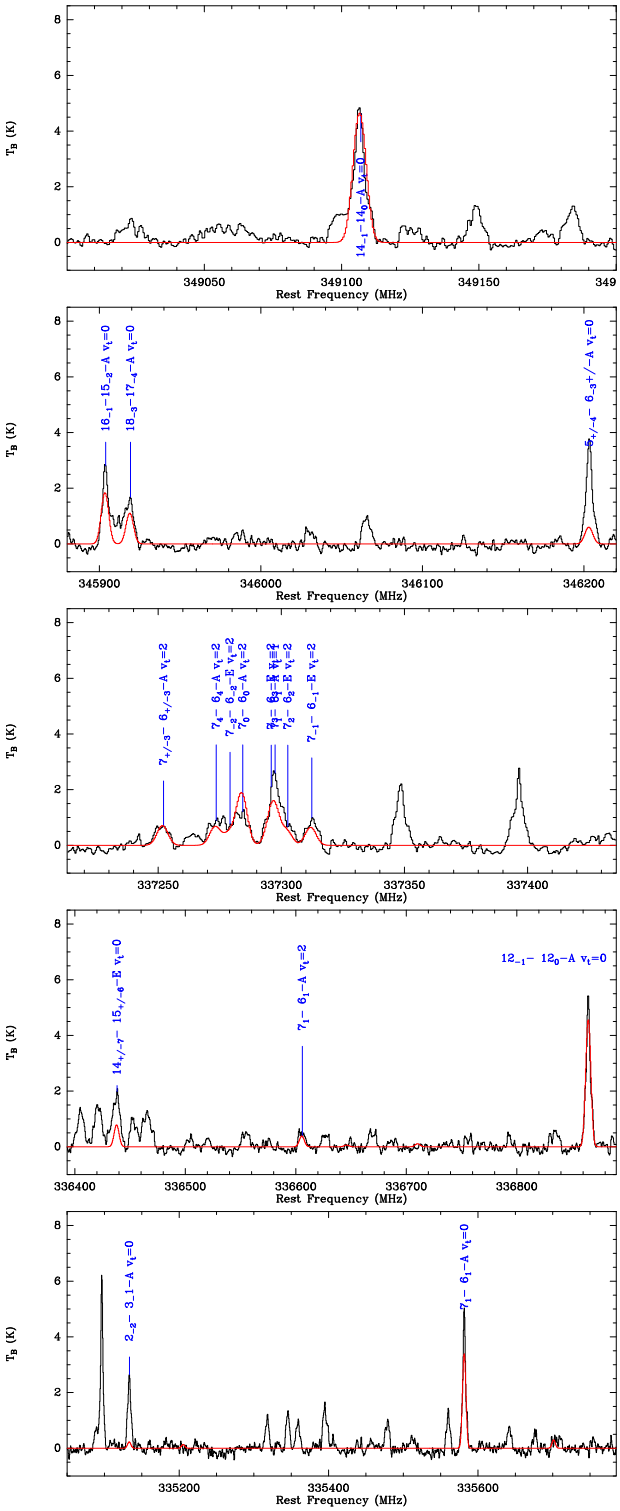

Fig. 2. Zoom-in of the different regions of the spectrum shown in Fig. A.1. The best-fit LTE CH_3OH synthetic spectrum is displayed in red and overlaid on the observed spectrum shown in black. The rest frequency of the fitted CH_3OH transitions listed in Table A.1 are labelled in blue.

3.1. High-excitation CH_3OH emission

Figure 1 shows the integrated intensity emission of the $7_1 - 6_1$-$A, v_t = 0$ line; integrated maps of other lines not affected by severe overlapping with other spectral features are shown in Fig. A.2. The emission is clearly compact and indeed traces the

Table 1. Results of the *uv* fit of the averaged[a] visibilities of CH_3OH lines[b] .

Transition	$\Delta\alpha^c$ (mas)	$\Delta\delta^c$ (mas)	FWHM[d]	P.A.[e]
$7_1 - 6_1$-$A, v_t = 0$	-12	+0	$0\farcs26 \times 0\farcs19$	36°
$12_{-1} - 12_0$-$A, v_t = 0$	-19	+0	$0\farcs23 \times 0\farcs16$	32°
$14_{-1} - 14_0$-$A, v_t = 0$	-7	+12	$0\farcs20 \times 0\farcs14$	16°

Notes. [(a)] Averaged over [-2,+2] km s^{-1} from the peak. [(b)] The resulting error on the centroid position is a function of the channel signal-to-noise ratio and atmospheric seeing, and is typically much smaller than the beam size. [(c)] Offsets are with respect to the peak of the continuum emission. Uncertainties are ∼ 4 mas. [(d)] Uncertainties are ∼ 30 mas. [(e)] Uncertainties are ∼ 10° − 18°.

inner region close to the protostar. We averaged the visibilities over the range ±2 km s^{-1} from the peak velocity of the $7_1 - 6_1$-$A, v_t = 0$, $12_{-1} - 12_0$-$A, v_t = 0$, and $14_{-1} - 14_0$-$A, v_t = 0$ lines to determine the size of the emitting region assuming an elliptical Gaussian distribution in space using the GILDAS *uv*-fit task. These lines are the strongest and most isolated in our dataset and are therefore less affected by blending with other transitions. The ±2 km s^{-1} velocity range minimises blending with a spectral feature at red-shifted velocities for the $14_{-1} - 14_0$-$A, v_t = 0$ line (Fig. 2). The fit gives a typical size of 0.″2 − 0.″3 (90 AU–135 AU in diameter, see Table 1 and Fig. 3) in good agreement with the estimate from CH_3CHO of Codella et al. (2016) with the same ALMA dataset. The position angles of the Gaussian fit are consistent within the errors with the position angle of the SiO jet (22°). This suggests that CH_3OH is associated with the jet/outflow system. Interestingly, the size of the emitting region seems to decrease going towards higher energies as found by Maury et al. (2014) in NGC 1333–IRAS2A for complex molecules. Since the analysed lines are the strongest of the dataset and have similar peak intensities, we believe that these results are not biased by different signal-to-noise levels.

To extract physical parameters from the data, a simultaneous fit was performed on the full spectrum. Weeds generates synthetic spectra of a given molecule assuming local thermodynamic equilibrium (LTE) over the full observed bandwidth. Since Weeds lacks an automatic optimisation algorithm we used MCWeeds (Giannetti et al. in prep.), an external interface between Weeds and PyMC (Patil et al. 2010), to implement Bayesian statistical models and fitting algorithms. We fit all CH_3OH transitions using the Markov chain Monte Carlo method. We used 100 000 iterations following a burn-in period of 20 000 with a thinning factor of 50. The source size was kept as a fixed parameter (0.″2, Table 1). Our analysis indicates that (i) CH_3OH is optically thin ($\tau \leq 0.4$), (ii) the best LTE fit temperature is well constrained to $\simeq$ 295 K, and (iii) the total column density at this temperature is $N_{CH_3OH} \simeq 3 \times 10^{17}$ cm^{-2}. The best fit results and the 95% highest probability density (HPD) interval ranges are given in Table A.2; the synthetic spectra corresponding to the best fit are shown in Fig. 2. The fit reproduces all lines except the $2_{-2} - 3_{-1}$-$A, v_t = 0$ and $5_{\pm4} - 6_{\pm3}$-$A, v_t = 0$ transitions which are underestimated by the model. These lines are among the lowest in energy in the dataset and likely trace a lower temperature regime than the other transitions.

The bolometric luminosity of HH 212 is ∼ 14 $L_\odot$ (Zinnecker et al. 1992). Using Eq. 1 of Ceccarelli et al. (2000), the dust temperature would be about 250 K at a radius of 10 AU, a factor of 5 lower than the size inferred from the present data. This suggests that the gas is thermally decoupled from dust, as was found for the inner regions of low-mass protostellar envelopes (e.g., Ceccarelli et al. 1996; Crimier et al. 2009) and/or that the CH_3OH excitation is enhanced by absorption of the IR radiation field. Indeed, Leurini et al. (2007b) showed that CH_3OH $v_t = 1$ lines trace the IR radiation field of the protostar (see their Fig. 3b): they zoom into the inner region around the YSO until the radius at which the dust becomes optically thick. Moreover, the size of ∼ 0.″2 is based on the *uv* fit of three low-energy lines. Higher energy lines, like those that drive the LTE fit of CH_3OH here, likely trace a more compact region. We note that a smaller source size would result in a similar temperature and a larger column density in the LTE fit since lines are optically thin.

3.2. CH_3OH kinematics

To study the kinematics of the hot gas traced by CH_3OH, we performed fits of the visibilities for various velocity channels for the $7_1 - 6_1$-$A, v_t = 0$ and $12_{-1} - 12_0$-$A, v_t = 0$ lines assuming that the emission follows an elliptic Gaussian distribution in space. In this case, we excluded the $14_{-1} - 14_0$-$A, v_t = 0$ transition because of blending (Fig. 2). The distributions of the velocity centroids are shown in Fig. 4. In the following, we assume a systemic velocity, V_{sys}, of +1.7 km s^{-1} (Lee et al. 2014). The lines have a clear velocity gradient in a direction parallel and very close to the equatorial plane. The high-velocity channels of the $7_1 - 6_1$-$A, v_t = 0$ line (and to some extent also of the $12_{-1} - 12_0$-$A, v_t = 0$ line) move out of the equatorial plane in the direction of the red-shifted lobe of the jet. In Fig. 3 we compare the centroid positions of the velocity channels of the $7_1 - 6_1$-$A, v_t = 0$ line with those of $C^{17}O$(2–1). CH_3OH behaves very differently from $C^{17}O$: at low velocities (± 1.5 km s^{-1}, from V_{sys}) $C^{17}O$ traces rotating envelope/outflow cavities, while at higher velocities (up to ± 3 km s^{-1}) it moves on the equatorial plane and shows a velocity pattern compatible with Keplerian rotation around a 0.2 − 0.3 $M_\odot$ YSO (Lee et al. 2014; Codella et al. 2014). On the contrary, for the two CH_3OH lines analysed here, the blue- and red-shifted velocity centroids are shifted roughly symmetrically on either side of the jet axis, indicating that the line-of-sight velocity beyond ∼ 0.7 km s^{-1} from systemic is dominated by rotational motions. The fact that this rotation velocity increases moving away from the protostar further indicates that CH_3OH is not associated with a Keplerian disk or rotating-infalling cavity, and it is more likely associated with an outflow/jet system. This is supported by the elongation of the integrated emission with a PA close to the jet axis (Table 1), and by the fact that the blue-shifted centroids are clearly shifted above the disk mid plane (Fig. 4).

4. Discussion

The CH_3OH emission arises from a region of 100 − 150 mas (45–68 AU) in radius around the protostar (see Table 1) and it is more compact than $C^{17}O$(2–1) (Fig. 3). This difference seems to rule out the association of CH_3OH with the cavities of the outflow traced by $C^{17}O$. Given the small size, CH_3OH could trace the base of the low-velocity outflow seen in SO (Podio et al. 2015). Codella et al. (2016) speculated that disk winds are present in this source based on the HDO emission, which hinted at optically thick emission from a very small (18–37 AU) and dense ($n \geq 10^9$ cm^{-3}) slow outflowing gas. Our analysis strengthens this scenario: CH_3OH originates from compact (solid upper limit of 135 AU to the diameter of the emitting region), hot ($T \sim 295$ K) gas elongated along the direction of the jet. We

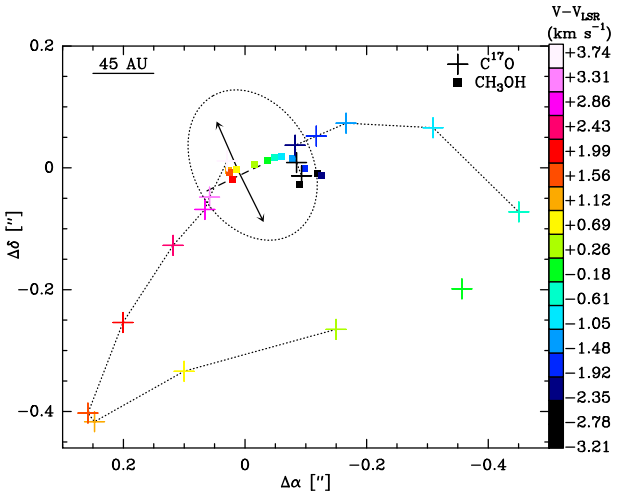

Fig. 3. Distribution of the centroid positions of various velocity channels of the 7_1–6_1-A, $v_t = 0$ line (squares) and of the $C^{17}O$(2–1) transition (crosses). Velocities are colour-coded according to the scale shown in the figure and are subtracted by the systemic velocity. The arrows indicate the direction of the jet; the dashed line traces the equatorial plane. For clarity, the $C^{17}O$(2–1) velocity channels are connected by dotted lines. The dotted ellipse represents the elliptical Gaussian fit to the averaged visibilities of the $7_1 - 6_1$-A, $v_t = 0$ line.

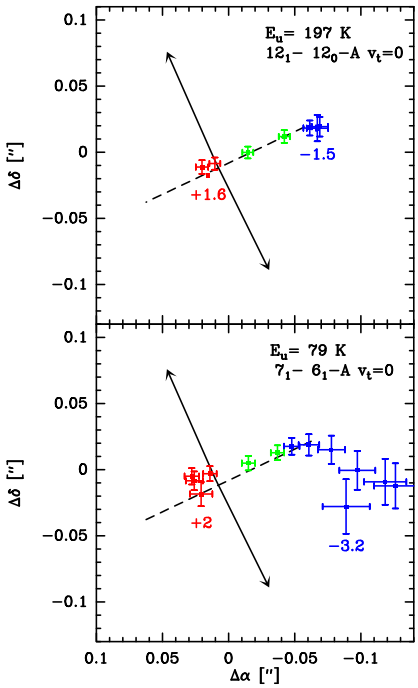

Fig. 4. Distribution of the centroid positions of various velocity channels of the $7_1 - 6_1$-A, $v_t = 0$ (bottom) and $12_{-1} - 12_0$-A, $v_t = 0$ (top) lines. In both panels, the velocity of the most blue- and red-shifted channels are subtracted by the systemic velocity. The velocity channels close to systemic velocity are marked in green. The arrows indicate the direction of the SiO jet; the dashed line traces the equatorial plane.

speculate that the observed velocities of CH_3OH are higher towards the outer part of the region than closer to the rotation axis (as expected in a disk wind model) because of beam dilution effects as described by Pesenti et al. (2004) for [OI]λ6300 data of the classical T Tauri star DG Tau. The fact that the velocity seems to increase at increasing distance from the source suggests that CH_3OH traces ejected gas rather than swept-up material. Interesting observations of high-mass YSOs (e.g., Sanna et al. 2015) show that IR-pumped Class II CH_3OH masers trace the outer launching region of the primary outflow. Higher angular resolution is necessary to investigate whether the SiO and the CH_3OH emission seen in HH 212 trace different velocity components of a nested onion-like system or two different physical structures. If CH_3OH is associated with an axisymmetric, steady, magneto-centrifugally accelerated disk wind, we can estimate its launching radius from Eq. 5 of Anderson et al. (2003). Assuming a poloidal velocity[1] of 30 km s^{-1} and a toroidal velocity of 1 km s^{-1} (Fig. 3) at some tens of AU from the axis, the launching radius is $\sim$ 1 AU, consistent with disk wind models of water in Class 0 YSOs (Yvart et al. 2016).

5. Conclusions

A simple cartoon (not to scale) of the inner region of HH 212 is given in Fig. A.3. The bulk of the $C^{17}O$ emission traces the protostellar envelope ($\sim$ 460 AU) flattened in the equatorial plane. Low-velocity $C^{17}O$ is associated with rotating cavity walls carved by the large scale outflow. The primary jet is shown by the SiO emission (and also detected at high-velocity in CO(3–2) and SO, Lee et al. 2015; Podio et al. 2015). We speculate that CH_3OH and HDO come from a compact ($<$ 135 AU in diameter) warm ($T \sim 295$ K) region likely associated with a disk wind gas accelerated at the base. Indeed, HDO and CH_3OH have similar peak velocities ($\sim$ 2 km s^{-1}) and line-widths (4–5 km s^{-1}). If CH_3OH traces a steady, axisymmetric, magneto-centrifugally driven disk wind, the launching region is at a radius of $\sim$ 1 AU from the YSO.

[1] For a maximum velocity CH_3OH of +2 km s^{-1} and an inclination angle of $\sim 4°$ to the plane of the sky (Claussen et al. 1998)

Acknowledgements. The authors thank the referee for the comments that have helped improve the clarity of the paper. S.L. acknowledges fruitful discussions with A. Sanna and F. Fontani. This paper makes use of the following ALMA data: ADS/JAO.ALMA#2011.0.000647.S. ALMA is a partnership of ESO (representing its member states), NSF (USA), and NINS (Japan), together with NRC (Canada), NSC and ASIAA (Taiwan), and KASI (Republic of Korea), in cooperation with the Republic of Chile. The Joint ALMA Observatory is operated by ESO, AUI/NRAO, and NAOJ.

References

Anderson, J. M., Li, Z.-Y., Krasnopolsky, R., & Blandford, R. D. 2003, ApJ, 590, L107
Cabrit, S., Codella, C., Gueth, F., & Gusdorf, A. 2012, A&A, 548, L2
Cabrit, S., Codella, C., Gueth, F., et al. 2007, A&A, 468, L29
Ceccarelli, C., Castets, A., Caux, E., et al. 2000, A&A, 355, 1129
Ceccarelli, C., Hollenbach, D. J., & Tielens, A. G. G. M. 1996, ApJ, 471, 400
Claussen, M. J., Marvel, K. B., Wootten, A., & Wilking, B. A. 1998, ApJ, 507, L79
Codella, C., Cabrit, S., Gueth, F., et al. 2007, A&A, 462, L53
Codella, C., Cabrit, S., Gueth, F., et al. 2014, A&A, 568, L5
Codella, C., Ceccarelli, C., Cabrit, S., et al. 2016, A&A, 586, L3
Crimier, N., Ceccarelli, C., Lefloch, B., & Faure, A. 2009, A&A, 506, 1229
Lee, C.-F., Hirano, N., Palau, A., et al. 2009, ApJ, 699, 1584
Lee, C.-F., Hirano, N., Zhang, Q., et al. 2014, ApJ, 786, 114
Lee, C.-F., Hirano, N., Zhang, Q., et al. 2015, ApJ, 805, 186
Lee, C.-F., Ho, P. T. P., Beuther, H., et al. 2006, ApJ, 639, 292
Lee, C.-F., Ho, P. T. P., Bourke, T. L., et al. 2008, ApJ, 685, 1026
Lee, C.-F., Ho, P. T. P., Hirano, N., et al. 2007, ApJ, 659, 499
Leurini, S., Beuther, H., Schilke, P., et al. 2007a, A&A, 475, 925
Leurini, S., Schilke, P., Wyrowski, F., & Menten, K. M. 2007b, A&A, 466, 215
Maret, S., Belloche, A., Maury, A. J., et al. 2014, A&A, 563, L1
Maret, S., Hily-Blant, P., Pety, J., Bardeau, S., & Reynier, E. 2011, A&A, 526, A47
Maury, A. J., Belloche, A., André, P., et al. 2014, A&A, 563, L2

Murillo, N. M., Lai, S.-P., Bruderer, S., Harsono, D., & van Dishoeck, E. F. 2013, A&A, 560, A103
Ohashi, N., Saigo, K., Aso, Y., et al. 2014, ApJ, 796, 131
Patil, A., Huard, D., & Fonnesbeck, C. 2010, JStatSoft, 35, 1
Pesenti, N., Dougados, C., Cabrit, S., et al. 2004, A&A, 416, L9
Pickett, H. M., Poynter, I. R. L., Cohen, E. A., et al. 1998, Journal of Quantitative Spectroscopy and Radiative Transfer, 60, 883
Podio, L., Codella, C., Gueth, F., et al. 2015, A&A, 581, A85
Price, D. J. & Bate, M. R. 2007, Ap&SS, 311, 75
Sakai, N., Sakai, T., Hirota, T., et al. 2014, Nature, 507, 78
Sanna, A., Surcis, G., Moscadelli, L., et al. 2015, A&A, 583, L3
Tobin, J. J., Hartmann, L., Chiang, H.-F., et al. 2012, Nature, 492, 83
Yvart, W., Cabrit, S., Pineau des Forêts, G., & Ferreira, J. 2016, A&A, 585, A74
Zinnecker, H., Bastien, P., Arcoragi, J.-P., & Yorke, H. W. 1992, A&A, 265, 726

Table A.1. List of CH_3OH transitions identified towards the position of the HH 212-mm protostar.

Transition	ν^a (MHz)	$E_{up}{}^a$ (K)	$A_{i,j}{}^a$ (10^{-4} s^{-1})
$2_{-2} - 3_{-1}$-A, $v_t = 0$	335133.570	44.7	0.27
$7_1 - 6_1$-A, $v_t = 0$	335582.017	79.0	1.63
$14_{\pm}7 - 15_{\pm}6$-A, $v_t = 0$	336438.224	488.2	0.36
$7_1 - 6_1$-A, $v_t = 2$	336605.889	747.4	1.64
$12_{-1} - 12_0$-A, $v_t = 0$	336865.149	197.1	2.04
$7_{-3} - 6_{-3}$-A, $v_t = 2$	337252.172	722.8	1.39
$7_3 - 6_3$-A, $v_t = 2$	337252.173	722.8	1.39
$7_4 - 6_4$-A, $v_t = 2$	337273.561	679.3	1.13
$7_{-2} - 6_{-2}$-E, $v_t = 2$	337279.180	709.7	1.54
$7_0 - 6_0$-A, $v_t = 2$	337284.320	573.0	2.29
$7_3 - 6_3$-E, $v_t = 2$	337295.913	686.2	1.37
$7_1 - 6_1$-A, $v_t = 1$	337297.484	390.0	1.66
$7_2 - 6_2$-E, $v_t = 2$	337302.644	651.0	1.55
$7_{-1} - 6_{-1}$-E, $v_t = 2$	337312.360	596.8	1.65
$16_{-1} - 15_{-2}$-A, $v_t = 0$	345903.916	332.7	0.90
$18_{-3} - 17_{-4}$-E, $v_t = 0$	345919.260	459.4	0.70
$5_{-4} - 6_{-3}$-A, $v_t = 0$	346202.719	115.2	0.22
$5_4 - 6_3$-A, $v_t = 0$	346204.271	115.2	0.22
$14_{-1} - 14_0$-A, $v_t = 0$	349106.997	260.2	2.20

Notes. [a] From the JPL database (Pickett et al. 1998)

Table A.2. Methanol LTE fit results

	Best Fit	95% HPD
Temperature (K)	295	290–300
Column density (10^{17} cm^{-2})	3.1	3.0–3.2
Source size ($''$)	0.2	—
Line-width (km s^{-1})	4.6	4.5–4.7
Peak velocity (km s^{-1})	2.1	2.0–2.1

Appendix A: Additional material

Table A.1 lists all methanol emission lines observed towards HH 212–MM1.

Table A.2 presents the best fit results and the 95% highest probability density (HPD) interval ranges.

Figure A.1 shows the full spectrum (both upper side band (USB), top panel, and lower side band (LSB), lower panel) extracted at the position of the HH 212-MM1 protostar. The horizontal red lines mark the regions of the spectrum plotted in Fig. 2 where the majority of methanol lines are found.

Figure A.2 shows the maps of the integrated line intensity of different methanol lines not affected by blending with other transitions. Figure A.3 summarises the scenario proposed for the inner region of the HH 212 protostellar system (not to scale).

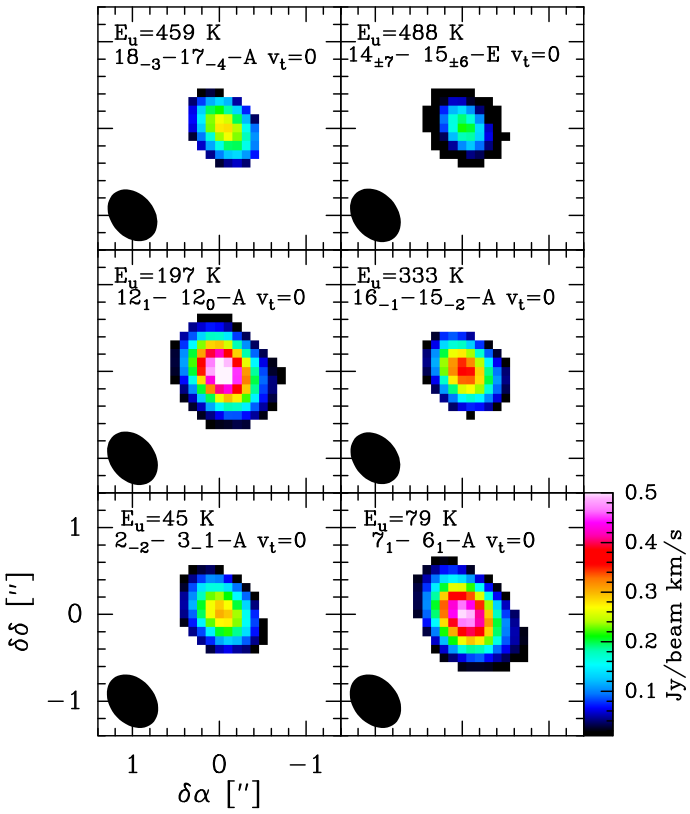

Fig. A.2. Integrated intensity maps of different methanol transitions. In each panel, the filled ellipse shows the synthesised beam of the corresponding map. To identify the lines, the upper energy of each transition is also indicated.

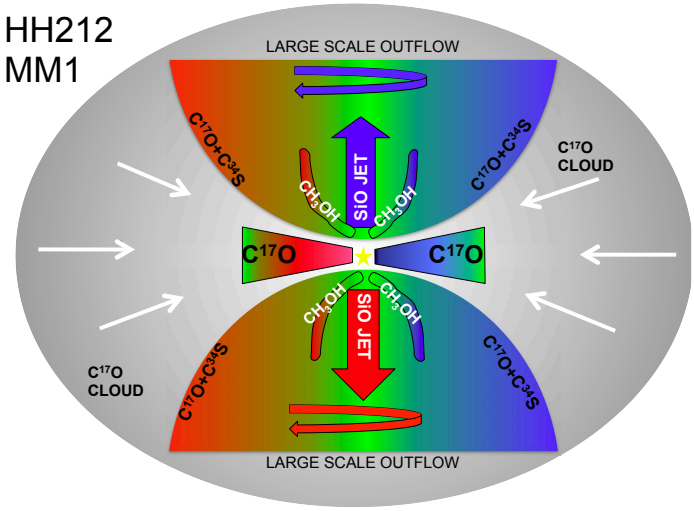

Fig. A.3. Cartoon (not to scale) illustrating the scenario proposed for the inner region of the HH 212 protostellar system based on the results presented in this paper and by Codella et al. (2014).

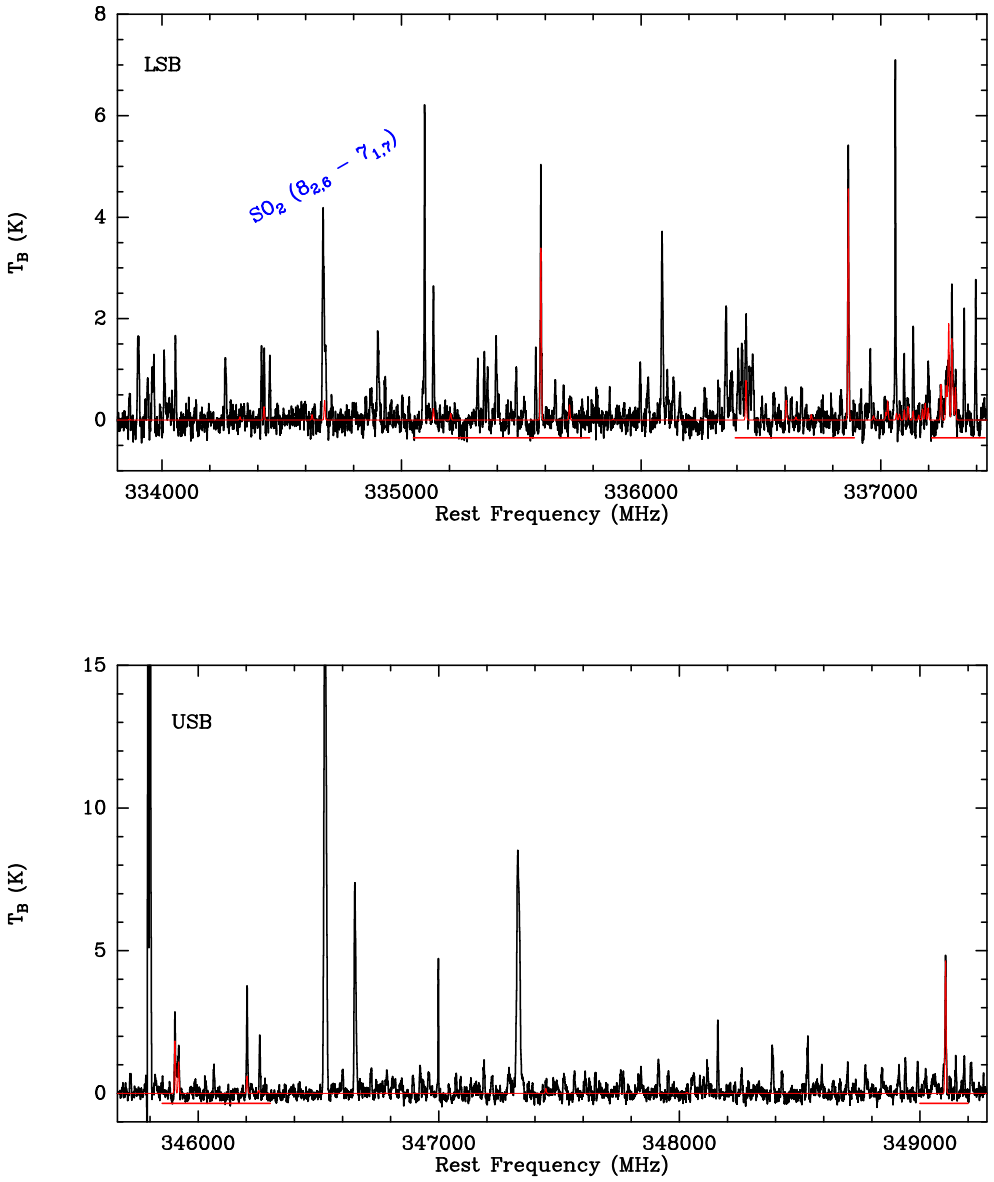

Fig. A.1. Full spectrum extracted at the dust peak position HH 212-MM1 (top panel: lower side band data; lower panel: upper side band data). The horizontal red lines mark the regions of the spectrum plotted in Fig. 2 where most of the methanol lines are found. The best fit LTE synthetic spectrum of methanol is displayed in red over the full 8 GHz bandwidth. In the upper panel, the $SO_2(8_{2,6} - 7_{1,7})$ is marked because it overlaps with a CH_3OH line (the $25_{-3} - 24_{-2} - E$, $v_t = 1$ transition, E_u= 1078 K). This methanol line was not included in the fit.